Simulation of vertical core-annular flow with a turbulent annulus

Li, Haoyu; Pourquié, M. J.B.M.; Ooms, G.; Henkes, R. A.W.M.

DOI
10.1016/j.ijmultiphaseflow.2023.104551

Publication date
2023

Document Version
Final published version

Published in
International Journal of Multiphase Flow

International Journal of Multiphase Flow 167 (2023) 104551

Contents lists available at ScienceDirect

International Journal of Multiphase Flow

journal homepage: www.elsevier.com/locate/ijmulflow

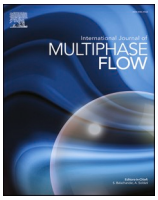

Simulation of vertical core-annular flow with a turbulent annulus

Haoyu Li *, M.J.B.M. Pourquié, G. Ooms, R.A.W.M. Henkes

Delft University of Technology, The Netherlands

ARTICLE INFO

Keywords:
Core-annular flow
RANS versus DNS
interfacial waves
Fanning friction factor
Hold-up ratio

ABSTRACT

The Reynolds-Averaged Navier Stokes (RANS) with the Launder & Sharma low-Reynolds number $k-\varepsilon$ model was used to simulate core-annular flow in the same configuration with vertical upflow as considered by Kim & Choi (2018), who carried out Direct Numerical Simulations (DNS), and by Vanegas Prada (1999), who performed experiments. The DNS are numerically very accurate and can thus be used for benchmarking of the RANS turbulence model. There is a large ratio between the oil and water viscosities, and the density difference between the water and oil is only small. The frictional pressure drop was fixed and the water holdup fraction was varied. Differences between the RANS and DNS predictions, e.g. in the wave structure and in the Reynolds stresses, are discussed. Despite the shortcomings of the considered Launder & Sharma low-Reynolds number $k-\varepsilon$ model in RANS, in comparison to DNS, the RANS approach properly describes the main flow structures for upward moving core-annular flow in a vertical pipe, like the travelling interfacial waves in combination with a turbulent water annulus. The Fanning friction factor with RANS is 18% lower than with DNS, and the holdup ratio with RANS is only slightly higher than with DNS (i.e. it has a slightly larger tendency to accumulate water in RANS than in DNS).

1. Introduction

For the transport of two-phase flow of immiscible fluids (like gas-liquid flow or liquid-liquid flow) through a horizontal or inclined pipe, different flow patterns can be distinguished. The prevailing flow pattern depends on a number of parameters, such as the pipe diameter and inclination, the flow rates of the two phases, and thermodynamic parameters of the phases, namely density, viscosity, and interfacial tension. When a very viscous liquid (like heavy oil) is combined with the flow of a certain amount of less-viscous liquid (like water), the so-called core-annular flow regime can occur. Here the oil is flowing in the centre of the pipe ("core flow"), and the water is flowing as a lubricating film ("annular flow") along the wall of the pipe. In this way the high pressure drop that would be found if only the viscous oil was flowing through the pipe is significantly reduced, as now not the oil viscosity but the water viscosity determines the pressure drop. This makes core-annular flow an attractive technology for viscous oil transport. Possible applications are in the petrochemical industry and in the food industry. In addition, core-annular flow is also of high interest from a fundamental fluid mechanics view point. An overview of core-annular flow has been given by Joseph et al. (1997) and Ghosh et al. (2009).

Over the past decades quite some studies were devoted to core-annular flow. This included small scale lab experiments in horizontal pipe flow or in a vertically upward going flow, and theoretical studies to determine the wave growth at the liquid-liquid interface. Most of the studies considered a laminar annulus flow (in addition to the laminar core flow). However, if the annulus-based Reynolds number is increased, the flow in the lubricating film will become turbulent. This will add complexity due to the interaction between the turbulence in the lubricating annulus and the travelling waves at the liquid-liquid interface. Some authors have applied a Reynolds-Averaged Navier-Stokes (RANS) approach, with a $k-\varepsilon$ model or a $k-\omega$ model for turbulence. See e.g. Ghosh et al. (2010), Shi et al. (2017), Ingen Housz et al. (2017), and Li et al. (2021, 2022).

Recently a first very detailed study was published by Kim & Choi (2018), who have carried out Direct Numerical Simulations (DNS) for vertical upflow in the core-annular flow regime with a laminar oil core and a turbulent annulus flow. The pipe diameter is 27.6 mm. The dynamic viscosity ratio between the two liquids was large (17600), but the density difference between the two liquids was only small (35 kg/m^3). Due to the small density difference, gravity almost does not play a role (note that there is no difference in flow in a horizontal or vertical pipe if the density of the two liquids is the same). Different values of the water holdup fraction in the pipe were simulated (i.e. different thicknesses of

* Corresponding author.
E-mail address: h.li-6@tudelft.nl (H. Li).

https://doi.org/10.1016/j.ijmultiphaseflow.2023.104551
Received 16 August 2022; Received in revised form 19 March 2023; Accepted 19 June 2023
Available online 20 June 2023

the annulus). Experiments for this configuration were carried out by Vanegas Prada (1999) and Vanegas Prada & Bannwart (2001). Due to the availability of DNS and experiments, this configuration can serve as an attractive case for benchmarking of turbulence models. Through grid refinement the DNS were shown to be very accurate, and they thus form the most accurate representation of the physics, as described by the Navier-Stokes equations. As the RANS approach contains closures for the turbulence (and DNS not), the RANS solution under transitional or turbulent flow conditions will be less accurate than DNS.

In the present study we have used RANS in the OpenFoam CFD package, with the Launder & Sharma low-Reynolds number $k-\varepsilon$ model, to simulate core-annular flow in the same vertical pipe configuration as considered by Kim & Choi (DNS) and by Vanegas Prada (experiments). We have recently also used the same RANS approach for core-annular flow in some different configurations (see Li et al, 2021, 2022). We have paid quite some attention to verifying that the RANS results are numerically accurate (through successive mesh refinement). As the RANS results will be axi-symmetric, 2D unsteady simulations were made. This will reveal the travelling waves at the oil-water interface with the turbulent water annulus. The RANS results will be compared with the DNS and experiments. Some remarkable differences in the results will be discussed.

The present study with RANS is valuable as this still is the most used approach in engineering simulations, as applied in the industry, through using third-party CFD packages or open-source CFD (like OpenFoam). This is because the computer time for RANS is much lower than for 3D DNS.

2. Modelling approach

2.1. Governing equations

The mass and momentum conservation equations for an incompressible, isothermal fluid are (in Cartesian coordinates):

$$\frac{\partial u_i}{\partial x_i} = 0 \tag{1}$$

$$\frac{\partial \rho u_i}{\partial t} + \rho u_j \frac{\partial u_i}{\partial x_j} = \frac{\partial}{\partial x_j}\left(\rho(\nu+\nu_t)\left(\frac{\partial u_i}{\partial x_j}+\frac{\partial u_j}{\partial x_i}\right)\right) - \frac{\partial p}{\partial x_i} + \rho g_i + F_{\sigma,i} \tag{2}$$

These are the Reynolds-Averaged Navier-Stokes Equations (RANS). Here u_i is the velocity, ρ and μ are the fluid density and viscosity, g_i is the gravitational acceleration, p is the pressure and $F_{\sigma,i}$ is the interfacial tension force. For the pipe flow, we will use $x_1 = x$ for the coordinate along the pipe axis, and $x_2 = y$ and $x_3 = z$ for the coordinates in the cross sectional plane; the velocity components are u, v, and w, in the directions x, y, and z, respectively. The gravity components are: $g_1 = -g$, and $g_2 = g_3 = 0$, where g is the gravitational acceleration. The actual simulations were carried out using 2D axi-symmetric coordinates with the radius $r = \sqrt{y^2+z^2}$.

The turbulent viscosity is modelled with the low-Reynolds number $k-\in$ model of Launder & Sharma (1974), which reads as follows:

$$\nu_t = C_\mu f_\mu \frac{k^2}{\widetilde{\varepsilon}} \tag{3}$$

$$\frac{\partial k}{\partial t} + u_j \frac{\partial k}{\partial x_j} = \frac{\partial}{\partial x_j}\left(\nu + \frac{\nu_t}{\sigma_k}\right)\frac{\partial k}{\partial x_j} + \nu_t\left(\frac{\partial u_j}{\partial x_j}\right)^2 - \widetilde{\varepsilon} - D \tag{4}$$

$$\frac{\partial \widetilde{\varepsilon}}{\partial t} + u_j \frac{\partial \widetilde{\varepsilon}}{\partial x_j} = \frac{\partial}{\partial x_j}\left(\nu + \frac{\nu_t}{\sigma_\varepsilon}\right)\frac{\partial \widetilde{\varepsilon}}{\partial x_j} + C_1 f_1 \frac{\widetilde{\varepsilon}}{k}\nu_t\left(\frac{\partial u_j}{\partial x_j}\right)^2 - C_2 f_2 \frac{\widetilde{\varepsilon}^2}{k} + E \tag{5}$$

With $D = 2\nu\frac{\partial\sqrt{k}}{\partial x_j}\frac{\partial\sqrt{k}}{\partial x_j}$ and $E = 2\nu\nu_t\left(\frac{\partial^2 u_j}{\partial x_j^2}\right)^2$. The turbulent energy dissipation rate is $\varepsilon = \widetilde{\varepsilon} + D$. Furthermore, $C_\mu = 0.09$, C_1=1.44, C_2=1.92, σ_k=1.0, σ_ε=1.3, $f_\mu = \exp\left(\frac{-3.4}{\left(1+\frac{Re_t}{50}\right)^2}\right)$, f_1=1, $f_2 = 1 - 0.3\exp(-Re_t^2)$, $Re_t = \frac{k^2}{\varepsilon\nu}$. The boundary conditions at the wall are: k=0 and $\widetilde{\in} = 0$.

Quite a number of low-Reynolds number $k-\in$ formulations are available in the literature. A large advantage of the Launder-Sharma one is that the low-Reynolds number terms do not include the explicit distance to the closest wall. Instead, the parameter Re_t is used to incorporate the effect of turbulence damping when a wall is approached. In the same way, the model will incorporate the possible damping of turbulence when the oil-water interface is approached in core-annular flow. The low-Reynolds number $k-\in$ model is used everywhere in the domain, also in the laminar oil core. Because of the presence of the low-Reynolds number terms the model automatically relaminarizes in the viscous oil core (i.e. it gives zero turbulent viscosity).

2.2. Numerical method

We used the open-source package OpenFOAM to solve the RANS equations, applying the CLSVOF method for the interface capturing. The CLSVOF solver, which was developed by Yamamoto et al. (2017), is based on the interFoam Volume of Fluid (VOF) solver in OpenFOAM. The level set function is used to calculate the interfacial tension force. Starting from the VOF method, the volume fraction α is introduced to distinguish between the two fluid phases: $\alpha = 0$ is the oil phase, $\alpha = 1$ is the water phase, and $0 < \alpha < 1$ denotes the oil-water interface. Then the fluid density and viscosity in the equations are:

$$\rho = (1-\alpha)\rho_o + \alpha\rho_w \tag{6}$$

$$\mu = (1-\alpha)\mu_o + \alpha\mu_w \tag{7}$$

The subscript "o" refers to oil, and the subscript "w" refers to water. α is calculated from the following advection equation:

$$\frac{\partial \alpha}{\partial t} + \nabla\cdot(\alpha\vec{u}) + \nabla\cdot\left((1-\alpha)\alpha\vec{u}_r\right) = 0 \tag{8}$$

The third term on the left-hand side is the compressive term (with the divergence of the compressive flux); here $\vec{u}_r = \vec{u}_w - \vec{u}_o$. This term is meant to control the sharpness of interface.

The level set function Φ is defined as the distance from the interface, where the interface is the isoline with $\Phi = 0$. The initial value of the level set function Φ_o is obtained from the initialized volume-of-fluid field, where the interface is defined at $\alpha = 0.5$:

$$\Phi_0 = (2\alpha - 1)\Gamma \tag{9}$$

$$\Gamma = 0.75\Delta X \tag{10}$$

Here ΔX is the minimum mesh size near the interface. Thereafter the re-initialization equation is solved to turn the initial level set function into the distance from the interface:

$$\frac{\partial \Phi}{\partial \tau} = \mathrm{sign}(\Phi_0)(1 - |\nabla\Phi|) \tag{11}$$

Here $\tau = 0.1\Delta X$ is the iteration time step of Φ and the sign function denotes:

$$\mathrm{sign}(\Phi) = \begin{cases} 1 \ \Phi > 0, \ water \\ 0 \ \Phi = 0, \ interface \\ -1 \ \Phi < 0, \ oil \end{cases} \tag{12}$$

Then the interface tension force is calculated as:

$$\vec{F}_\sigma = \sigma\kappa(\Phi)\delta_\Phi\nabla(\Phi) \tag{13}$$

Here σ is the interface tension and δ_Φ is the smoothed delta function:

$$\delta_\Phi = \begin{cases} \frac{1}{2\gamma}\left(1+\cos\left(\frac{\pi\Phi}{\gamma}\right)\right) \ for \ |\Phi| < \varepsilon \\ 0 \ elsewhere \end{cases} \tag{14}$$

The quantity γ is the interface thickness coefficient (see Yamamoto

et al., 2017) and $\kappa(\Phi)$is the interface curvature:

$$\kappa(\Phi) = \nabla \cdot \vec{n}_c \tag{15}$$

$$\vec{n}_c = \frac{(\nabla\Phi)_f}{\left|(\nabla\Phi)_f\right|} \tag{16}$$

Here $\vec{n}_c$ is the surface unit normal vector. The contact angle θ between the interface and the pipe wall is defined as:

$$\cos(\theta) = \vec{n}_c \cdot \vec{n}_w \tag{17}$$

With $\vec{n}_w$ being the unit normal vector at the wall. The contact angle is set to 90^o in our simulations. This means that both the level set function Φ and the volume fraction of the fluid α satisfy the zero-gradient condition at the pipe wall boundary.

A pressure drop in the flow direction is added as an extra force term to the right-hand side of Eq. (2), with periodic boundary conditions on the left and right side of the pipe. Therefore, the pressure that remains in the equations is periodic with respect to the left and right side of the computational pipe section. The initially assumed velocity profile will then develop over time under this pressure drop in the transient simulation until a stable state is obtained.

A second-order backward implicit time discretization scheme is applied, with a very small time step (small Courant number). This gives a very accurate time integration. We use a second-order scheme for the advection terms in the momentum equations and in the interface equation (as used in the level set method), but a first-order upwind scheme for the advection in the equations for the turbulence quantities k and ε; trying a second-order scheme for the latter gave numerical instabilities. Through successive mesh refinement, however, we have verified that the simulation results are accurate (and not suffering from large numerical diffusion).

In all the simulations, periodic boundary conditions are applied at the inlet and outlet of the pipe section, which restricts the wavelengths in the axial direction to the domain length divided by an integer value. At the pipe wall, the no-slip condition is imposed. We have used the symmetric PBiCG solver for the velocity and for the turbulent quantities, the GAMG solver for the pressure, and the PIMPLE solver for the velocity-pressure coupling.

2.3. Key parameters

Four important parameters are: the total flow rate, the pressure drop, the watercut, and the water hold-up fraction. When two parameters are set as input (e.g. the total flow rate and the watercut in the experiments), the other two will follow as output.

The watercut is defined as the ratio of the water volumetric flow rate and the total volumetric flowrate:

$$\mathrm{WC} = Q_w/(Q_o + Q_w) \tag{18}$$

where Q denotes the volumetric flow rate. The water hold-up fraction is defined as the ratio of the in-situ water volume in the pipe and the total volume of oil and water:

$$\alpha_w = \frac{V_w}{V_w + V_o} \tag{19}$$

A related parameter is the so-called hold-up ratio h, which is defined as:

$$h = \frac{Q_o/Q_w}{V_o/V_w} \tag{20}$$

This can also be rewritten as $h = 1 + u_r/u_w$. Here the velocity difference $u_r = u_o - u_w$, is the apparent (average) slip velocity between the oil core (having a bulk velocity u_o) and the water annulus (having a bulk velocity u_w). Note that h=1 if there is no slip between the bulk oil and water velocities. The hold-up ratio thus is a measure of the apparent slip between the oil core and the water annulus.

2.4. Basic simulation set-up

The base conditions for the considered configuration are the same as those used in the lab experiments described by Vanegas Prada (1999) and Vanegas Prada & Bannwart (2001). The vertical pipe has a diameter of 27.6 mm. The oil and water densities are ρ_o=963 kg/m^3 and ρ_w=998 kg/m^3, and the oil and water viscosities are μ_o=17.6 Pa s and μ_w=0.001 Pa s. Therefore, the oil dynamic viscosity is 17600 times higher than the water value. The interfacial tension between oil and water is σ=0.03 N/m. In the DNS simulation by Kim & Choi different values of the water hold-up fraction are used: α_w= 0.09, 0.17, 0.29, 0.38, and 0.44. The imposed pressure drop in the simulations is such that the resulting wall shear stress corresponds to $Re_\tau = u_\tau R/\nu$ =720, which in fact means that the frictional pressure drop is equal to 400 Pa/m. The imposed full pressure drop is found by adding the hydrostatic head, which is $(\rho_w\alpha_w + \rho_o\alpha_o)g$ [Pa/m].

The experiments are described in detail in the Master Thesis by Vanegas Prada (1999), which also includes tables with the experimental results. The key measurements are the pressure drop as function of the oil and water flow rates. Through the measured oil and water flow rates also the watercut is known. The water hold-up fraction is α_w was not measured, though a value for it is included in the tables. It looks like a hold-up ratio of about h =1.1 has been assumed. The measurement points with a frictional pressure drop of (about) 400 Pa/m have been selected by Kim & Choi (2018) for their validation of the DNS. The same set of experiments will be used in the present study as well.

Time-dependent, 2D, axisymmetric RANS simulations were carried out for a pipe section with a length of 16.6 mm. Sensitivity simulations were made to investigate the effect of the chosen section length. Periodic boundary conditions are imposed between the start and end of the section. The pressure gradient is prescribed. The water hold-up α_w is imposed as initial condition, and the total water holdup fraction is conserved over time. The oil and water flow rates follow as output quantities. The simulation is started with a flat oil-water interface. Waves develop at the interface in the transient simulation. The simulation is continued over a sufficient long time such that fully developed flow with travelling interfacial waves has developed. Grid refinement was applied to verify that the simulation results are sufficiently numerically accurate. Thereto an equidistant grid was applied in streamwise direction (i.e. x-coordinate) and a non-equidistant grid in the radial direction (i.e. r-coordinate). The latter has a strong refinement close to the boundary layer along the pipe wall, where there are large radial gradients in the velocity profile.

It should be note that the difference in density between the oil and water is quite small, namely 35 kg/m^3, which is 3.5% of the water density. Therefore, the effect of the density difference on the core-annular flow will be very small, which was verified by the RANS simulations. This means that in fact, with good accuracy, gravity could have been omitted in the simulations.

2.5. Force balance

An integral force balance for the flow (after averaging in space and time) can be derived, using the quantities shown in Fig. 1. The global 3D flow structure (as measured by Bannwart et al., 2000) is reproduced in Fig. 1a. For the notations see Fig. 1b: here x is the streamwise pipe coordinate, and r is the radial pipe coordinate. The pipe has radius R. The oil flow is represented by a concentric core with radius R_c, and the water flows in an annulus with thickness $R - R_c$. The flow is driven by the pressure gradient $-dp/dx$.The wall imposes a wall shear stress τ_W on the water annulus (taken positive in upstream direction). The water annulus imposes an interfacial stress τ_i on the oil core (taken positive in upstream direction). The oil core also imposes an interfacial stress on the water

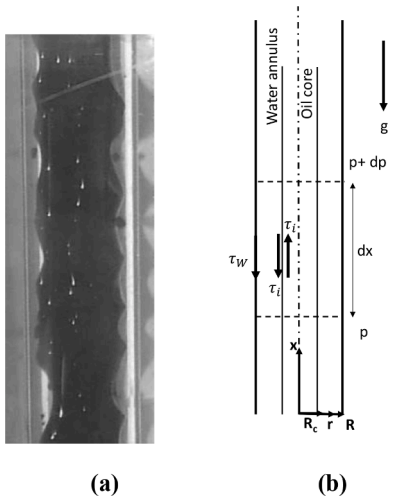

Fig. 1. Vertical core-annular flow; (a) snapshot from experiments (taken from Bannwart et al., 2000), (b) sketch of the forces.

annulus, which has the same magnitude as τ_i, but now taken positive in downstream direction. The water flows with an average velocity (bulk velocity) u_w, and the oil flow with an average velocity (bulk velocity) u_o. The bulk velocity follows from the superficial velocity as: $u_w = u_{sw}/\alpha_w$ and $u_o = u_{so}/\alpha_o$, with $u_{sw} = Q_w/A$ and $u_{so} = Q_o/A$. Here $A = \pi R^2$ is the cross-sectional area of the pipe. The bulk oil viscosity u_o can also be denoted as the core velocity u_{core}.The mixture velocity is defined as $u_m = u_{sw} + u_{so} = (Q_w + Q_o)/A$.

The force balance for the combined oil-water flow in a horizontal pipe reads:

$$-\frac{dp}{dx}A - \tau_W 2\pi R - (\rho_w \alpha_w + \rho_o \alpha_0) gA = 0 \tag{21}$$

The force balance for the oil core gives:

$$-\frac{dp}{dx}\alpha_o A - \tau_i 2\pi R_c - \rho_o g \alpha_0 A = 0. \tag{22}$$

Here α_o is the oil hold-up fraction, with $\alpha_o = (R_c/R)^2$.

From force balances (21) and (22) it also follows that the wall shear stress and interfacial stress are related as $\tau_i = \tau_W \left(\frac{R_c}{R}\right)\left(1 - \frac{1}{2}\left(1 - \left(\frac{R_c}{R}\right)^2\right)\left(\rho_w - \rho_{wo}\right) gR\right)$. Note that the force balances (21) and (22) hold for the core-annular flow (with or without interfacial waves) after averaging in space and time.

Due to the considered high ratio of the oil and water viscosities, the oil core will be laminar. Assuming parallel flow in the laminar oil core (i.e. neglecting non-parallel effects in the oil flow close to the wave interface), the core flow can be described by the force balance:

$$-\frac{dp}{dx}\pi r^2 - \mu_o \frac{du}{dr} 2\pi r - \rho_o g \pi r^2 = 0, \tag{23}$$

with the interface condition: $\tau_i = -\mu_o \left(\frac{du}{dr}\right)_{r=R_c}$.

Integration gives the following expression of the velocity at the interface:

$$u_i = -\frac{R_c}{4\mu_o}\tau_i + \frac{Q_o}{\pi R_c^2}, \tag{24}$$

in which Q_o is the oil flow rate. For all conditions considered in the present study, the first term on the right-hand side is much smaller than the second term. This means that within the boundaries of validity of the shown force-balance approach with parallel core flow, the interfacial velocity is the same as the bulk oil velocity.

3. RANS results

3.1. Water-only pipe flow

Various authors have carried out DNS for single-phase turbulent pipe flow up to high Reynolds numbers, such as Eggels et al. (1994), Wu & Moin (2008), Wu et al. (2012) and Pirozzoli et al. (2021). Accurate turbulent pipe experiments have been caried out by Den Toonder & Nieuwstadt (1997), for moderate Reynolds numbers, and by Zaragoza & Smits (1998), using the Princeton Superpipe up to very high Reynolds numbers. Predictions for the Fanning friction factor as function of the Reynolds number as obtained with the RANS model with the Launder & Sharma low-Reynolds number $k-\varepsilon$ model are compared with the DNS and experiments in Fig. 2 (the Reynolds number is based on the pipe diameter, bulk velocity, and kinematic fluid viscosity, i.e. $Re = uD/\nu$). The Fanning friction factor is defined as $f_W = -\left(\frac{dp}{dx}\right)\frac{R}{\rho u^2}$. The values in the DNS and experiments are very close to each other. RANS slightly underpredicts the friction factor, though the deviation becomes less for increasing Reynolds number. At about Re=27000, which is the (mixture) Reynolds number in the core-annular flow DNS by Kim & Choi, the RANS value of the friction factor is 0.0056, which is about 7% lower than the DNS and experimental value of 0.006.

Fig. 3 compares various quantities in turbulent pipe flow at Re=24580 as obtained from our RANS simulations and with the DNS by Wu & Moin (2008) and Wu et al. (2012). The DNS have a corresponding $Re_\tau = u_\tau R/\nu = 685$. The shown quantities (velocity, turbulent kinetic energy, Reynolds stress, and turbulent viscosity) have a plus superscript to indicate that they are non-dimensionalized with the wall shear velocity u_τ and the kinematic viscosity ν. The wall shear velocity u_τ is defined as $u_\tau = \sqrt{\tau_W/\rho_w}$, in which the wall shear stress is related to the frictional pressure drop as $\tau_W = -(dp/dx)\, R/2$. Fig. 3 shows that RANS and DNS for the velocity and Reynolds stress are in fairly close agreement, but the peak for the kinetic energy with RANS (k^+=3.2) is significantly below the DNS value k^+=4.7). The level of the turbulent viscosity ν_t^+ away from the wall is about 40 for the DNS and 60 for the RANS simulations.

3.2. Two-phase flow

3.2.1. Numerical accuracy and dependence on oil viscosity

The two-phase RANS simulations were carried out in a moving frame of reference, in which the wall has been given a velocity of 1 m/s, which

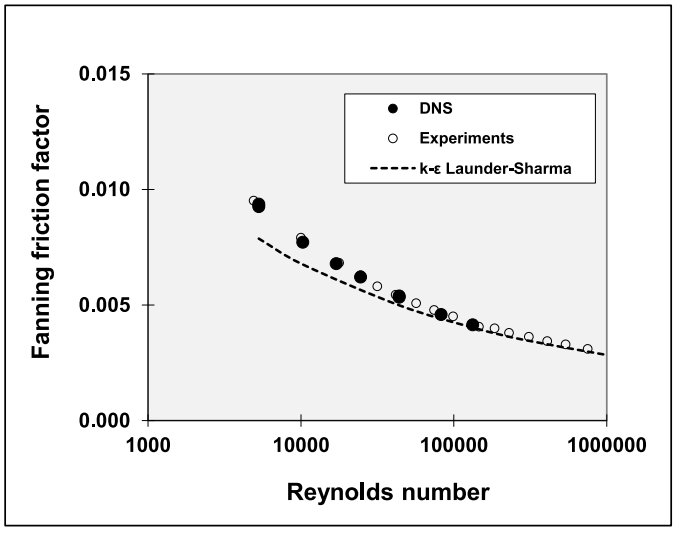

Fig. 2. Comparison of RANS, DNS, and experiments; Fanning friction factor as function of the Reynolds number for single-phase turbulent pipe flow.

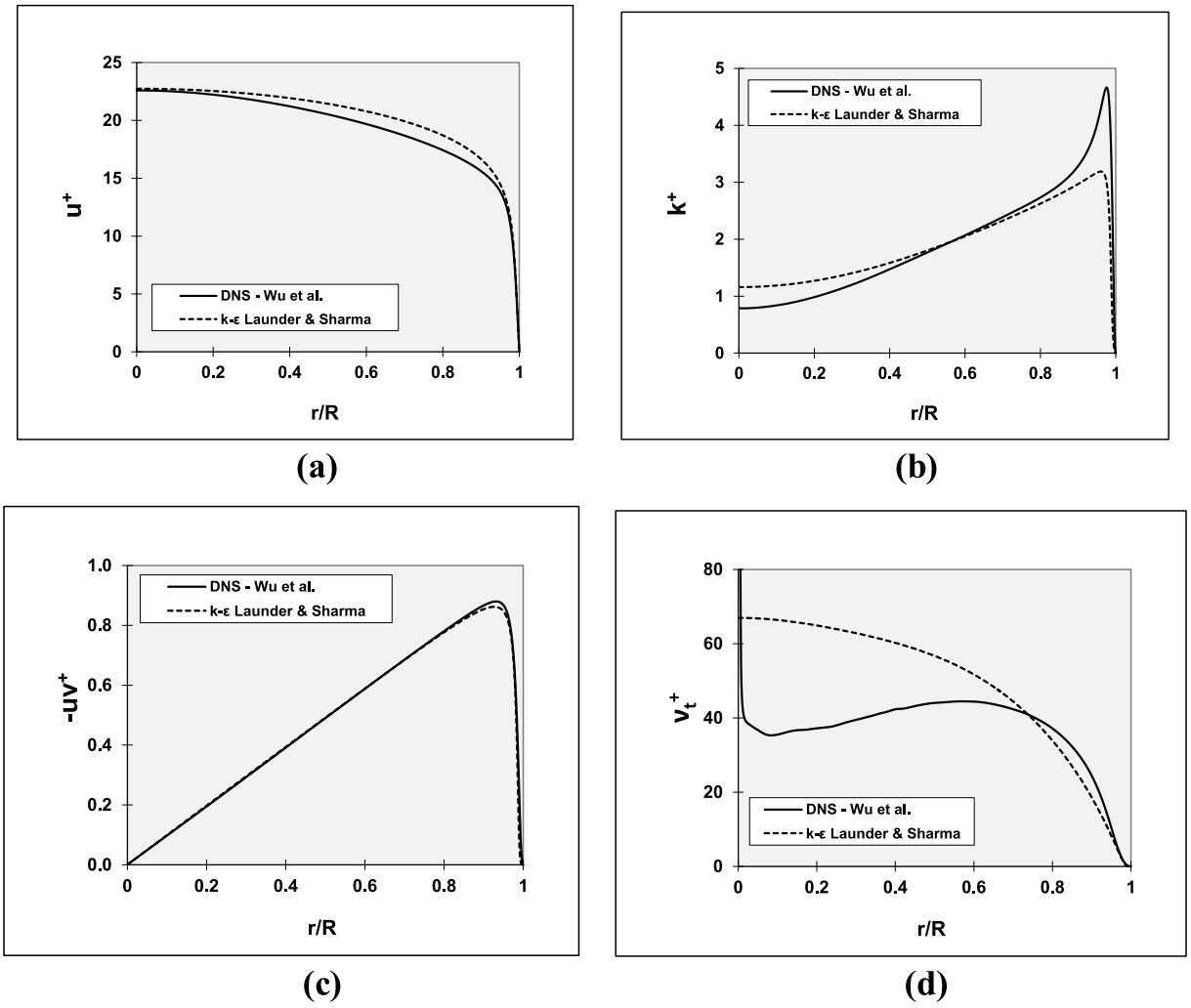

Fig. 3. RANS versus DNS for single phase turbulent pipe flow at Re=24600.

is close to the velocity of the interface waves. As a result, the waves in the moving frame of reference are almost stagnant, which helps to improve the numerical stability. Despite this, numerical instabilities remained if the oil viscosity was set to μ_o=17.6 Pa s, which is the same value as used in the lab experiments by Vanegas Prada (1999) and in the DNS by Kim & Choi (2018). Numerically stable and accurate solutions could be obtained if the oil viscosity was reduced to a value of the order 1 Pa s. This is significantly lower than the target value, though still very

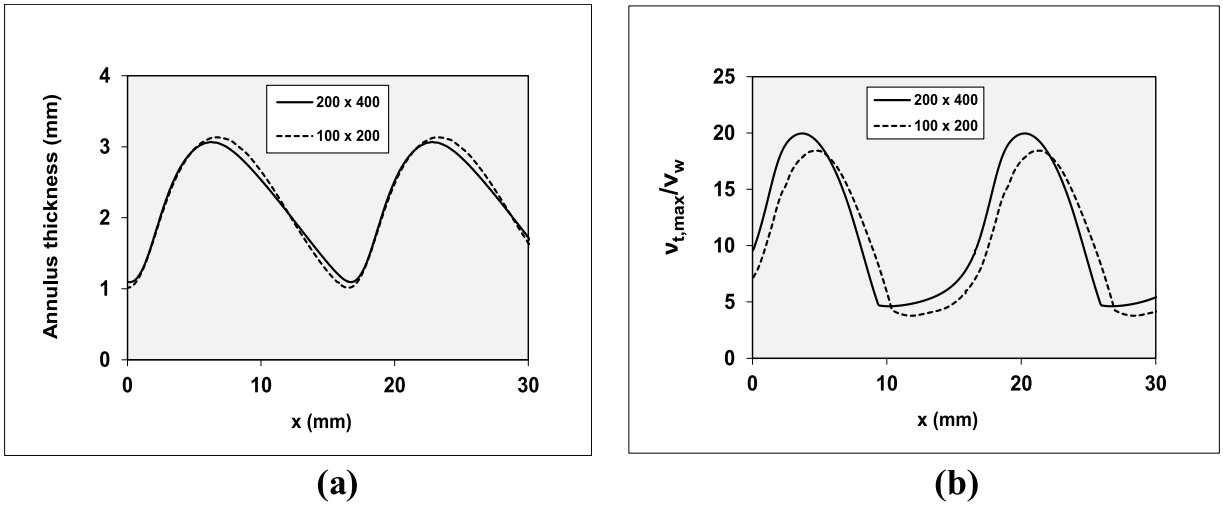

Fig. 4. RANS results for (a) annulus thickness, and (b) maximum turbulent viscosity (oil viscosity = 0.75 Pa s, water hold-up fraction = 0.29, section length = 16.6 mm, frictional pressure drop = 400 Pa/m).

much higher (by a factor 1000) than the water viscosity of 0.001 Pa s. Despite this difference, we think that the comparison between the RANS and DNS is meaningful. Moreover, we expect that other research groups will pick up the same case for benchmarking in the near future. Using a more advanced numerical code (e.g. inhouse academic code versus the applied OpenFoam code) may resolve the numerical issues at high oil viscosity.

The verification of the numerical accuracy of the results is of key importance. Given the complexity of the simulations, we think that a good numerical accuracy has been obtained. To demonstrate this, an example is given in Fig. 4 for μ_o=0.75 Pa s, which shows snapshots of the annulus thickness and the maximum turbulent viscosity. Numerical values are listed in Table 1 (which also includes the results for μ_o=0.46 and 1.5 Pa s. The length of the pipe section is set to 16.6 mm and a water hold-up fraction of 0.29 was used. The imposed frictional pressure drop is 400 Pa/m. The good accuracy of the numerical simulations is shown through comparing the results on a coarser 100×200 grid (i.e. 100 points in streamwise direction, and 200 points in radial direction) and on a refined 200×400 grid.

For μ_o=0.75 Pa s on the finer grid, the resulting mixture velocity is 1.07 m/s, and the watercut is 24%. The corresponding core velocity is 1.15 m/s. The wave velocity is slightly lower than the core velocity, namely 1.11 m/s. The wave frequency is 67 Hz (being equal to the ratio of the wave velocity and the section length). As shown in Fig. 4 for an oil viscosity μ_o=0.75 Pa s, the oscillation in the thickness of the water annulus and in the maximum turbulent viscosity in the water annulus on the 200×400 grid is close to the results on the coarser 100×200 grid. Fig. 5 shows (using the finer 400×200 grid) that the oscillation only slightly depends on the oil viscosity. Therefore, it makes good sense to compare the present RANS results with the DNS of Kim & Choi with the experiments by Vanegas Prada (1999), despite the latter two were obtained for an even higher oil viscosity.

3.2.2. Dependence on pipe section length

The base section length in the RANS simulations is L=16.6 mm. The effect of the section length on the interfacial waves was investigated by also simulating a section length of 2L and 3L. The numerical accuracy was verified by using both the 100×200 grid and the refined 200×400 grid. The considered conditions are: oil viscosity μ_o=0.75 Pa s, water hold-up fraction α_w =0.29, frictional pressure drop is 400 Pa/m. The different pipe sections all give a same mixture velocity of 1.07 m/s, and a watercut of 24% (corresponding to an average oil core velocity of 1.15 m/s). The wave velocity is between 1.05 and 1.11 m/s.

A snapshot of the thickness of the water annulus and of the maximum turbulent viscosity through the annulus thickness, as function of the streamwise pipe coordinate x, is shown in Fig. 6. A single wave length of 16.6 mm is found when choosing the base section length L=16.6 mm. When the section length is increased, the oscillation becomes more irregular, but the averaged wave length is still close to 16.6 mm, namely about 18 mm for 2L and 13 mm for 3L. The figure also shows that the turbulent viscosity is largest/smallest at the location where the thickness of the water annulus is (almost) largest/smallest.

This comparison shows that increasing the length of the pipe section will give a small change of the dominant frequency (or wave length), introducing a slight irregularity in the wave structure wave some non-periodicity. Using a pipe section of 16.6 mm with periodic boundary conditions gives a pure travelling wave. This can be seen as a relevant representation of the more complex transients at increased section length (giving a slight tendency to have a spectrum of waves rather than a pure single dominant wave).

3.2.3. Dependence on the water hold-up fraction

Various RANS simulations were carried out to determine the effect of the water hold-up fraction α_w. The considered conditions are: pipe section length is 16.6 mm, oil viscosity μ_o=0.75 Pa s, frictional pressure drop is 400 Pa/m. The simulated thickness of the water annulus and the maximum turbulent viscosity are shown in Fig. 7. As expected, the amplitude of interfacial waves increases when the water hold-up fraction is increased from 0.09 to 0.44. The wave length seen in the thickness of the water annulus is L=16.6 mm for the higher values of the water hold-up fraction (0.29, 0.38, and 0.44) though becomes half that value, i.e. $L/2$=8.4 mm, for the lower fraction (0.17, 0.09). The maximum turbulent viscosity decreases with decreasing water hold-up fraction, which means that the presence of a (thicker) oil core suppresses the turbulence. The value of the maximum turbulent viscosity is highest for water-only flow (i.e. α_w=1), namely $\nu_{t,max}/\ \nu_w$=67. For the smallest simulated value of the water hold-up fraction (α_w=0.09), the thickness of the water annulus is so small that the layer fully relaminarizes (i.e. $\nu_{t,max}/\ \nu_w$=0).

Fig. 8 shows a snapshot of the streamlines with respect to an observer that moves with about the wave velocity at the interface. In the next section, the RANS results for various values of the water hold-up fraction will also be used for comparison with the DNS of Kim & Choi (2018).

3.2.4. Dependence on gravity

The density difference between the water and oil is so small (only 35 kg/m^3 compared to a water density of 998 kg/m^3) that its effect on the vertical core annular flow is negligibly small. This is demonstrated for the RANS simulations (with oil viscosity μ_o= 0.75 Pa s) in Fig. 9. The simulations without and with gravity give almost the same results for the oscillation in the thickness of the water annulus and of the maximum turbulent viscosity. Results without and with gravity are also practically the same when the length of the pipe section is increased to 2L and 3L (i.e. results without gravity are almost the same as those with gravity in Fig. 6).

The DNS by Kim & Choi were only carried out with gravity. But it is very likely that also the DNS without gravity would be very close to the results with gravity. Thus, this test case is actually one with a difference in liquid viscosity, though with a negligible difference in density. In fact, this means that the results will be independent of the pipe inclination (vertical upflow is the same as horizontal flow, for an imposed frictional pressure drop of 400 Pa/m).

4. Comparison of RANS results with experiments and DNS

In this comparison we have closely followed the approach by Kim & Choi (2008). Reference is made to the experiments by Vanegas Prada (1999) and by Vanegas Prada & Bannwart (2001). The experiments only provide results for the pressure drop and water holdup fraction (as function of the mixture velocity and watercut. The experiments do not

Table 1
RANS results for different oil viscosities on different numerical grids (water hold-up fraction = 0.29, section length = 16.6 mm, frictional pressure drop 400 Pa/m).

	Grid	Mixture vel. m/s	Watercut %	Wave length mm	Wave velocity m/s	Wave frequency Hz
0.46	100 × 200	1.07	23	16.6	1.05	63
0.46	200 × 400	1.09	22	16.6	1.08	65
0.75	100 × 200	1.07	24	16.6	1.08	65
0.75	200 × 400	1.07	24	16.6	1.11	67
1.5	100 × 200	1.05	24	16.6	1.11	67
1.5	200 × 400	1	24	16.6	1.04	63

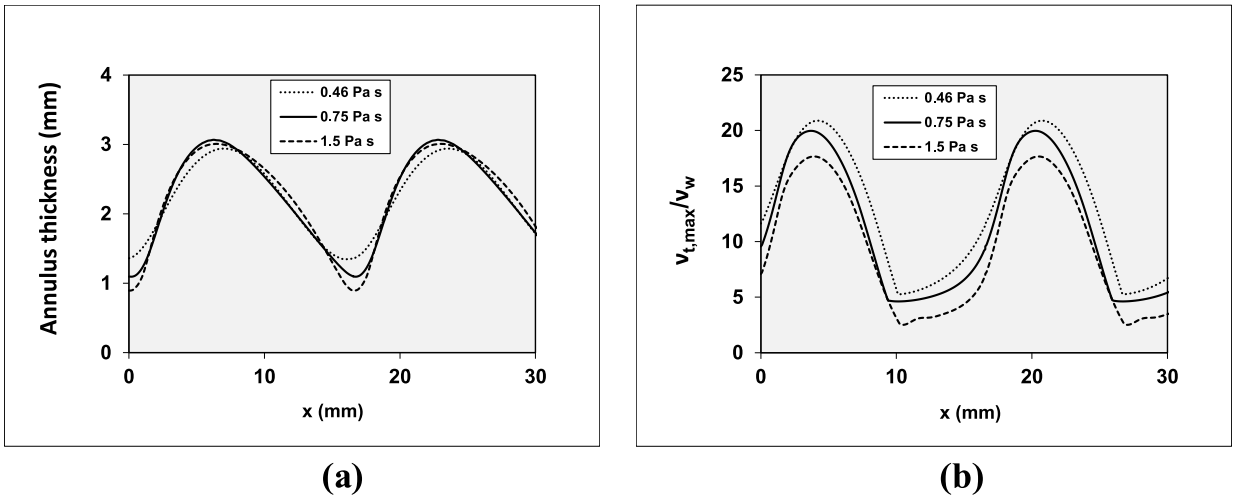

Fig. 5. RANS results with different oil viscosities for (a) annulus thickness, and (b) maximum turbulent viscosity; water hold-up fraction = 0.29, section length = 16.6 mm, frictional pressure drop = 400 Pa/m.

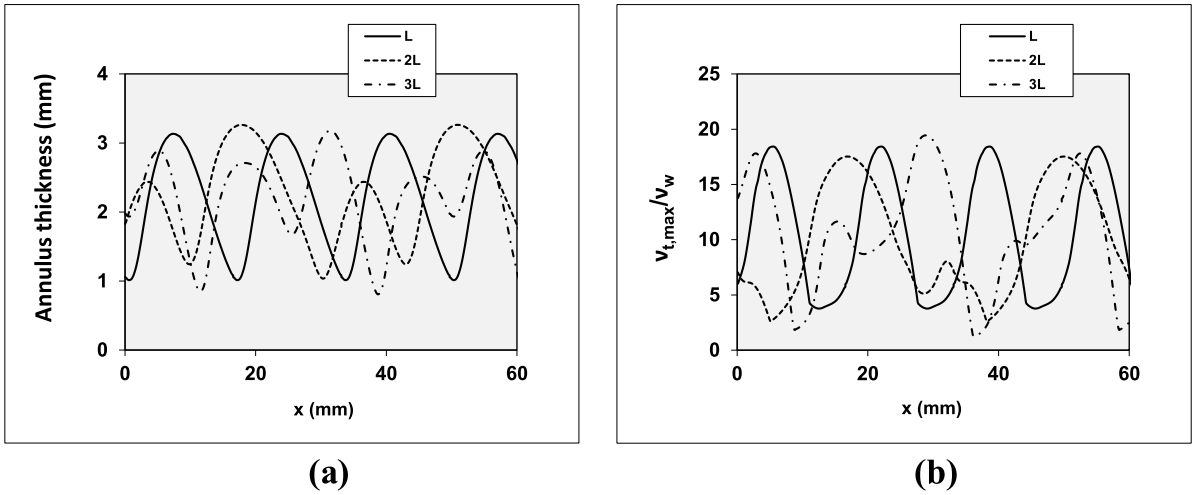

Fig. 6. RANS results with different pipe section lengths (values shown in legend, L=16.6 mm) for (a) annulus thickness, and (b) maximum turbulent viscosity; water hold-up fraction α_w= 0.29, oil viscosity is μ_o = 0.75 Pa s, frictional pressure drop is 400 Pa/m.

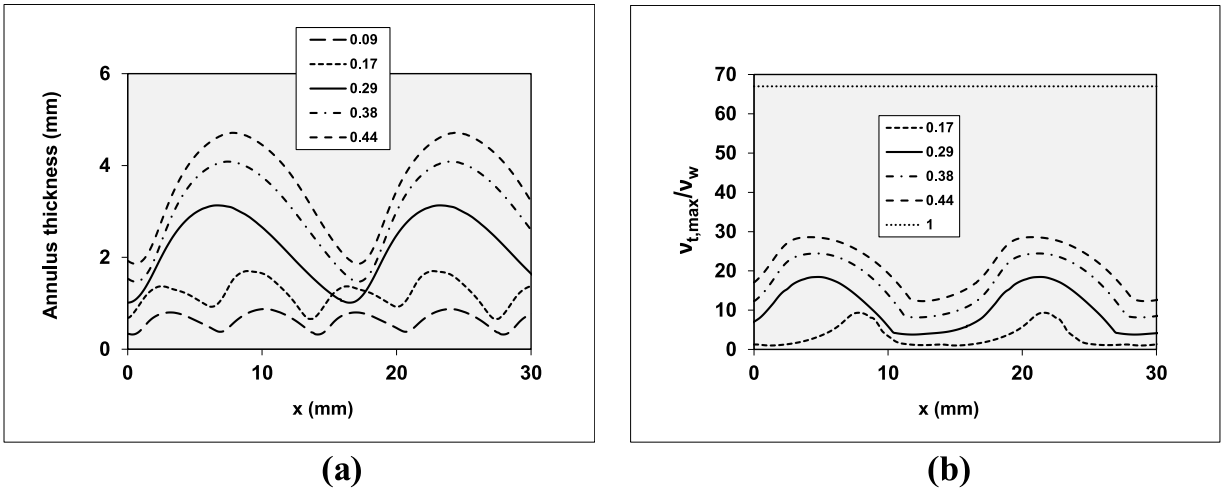

Fig. 7. RANS results with different water hold-up fraction (values shown in legend) for (a) annulus thickness, and (b) maximum turbulent viscosity; oil viscosity is μ_o= 0.75 Pa s, section length L= 16.6 mm, frictional pressure drop is 400 Pa/m.

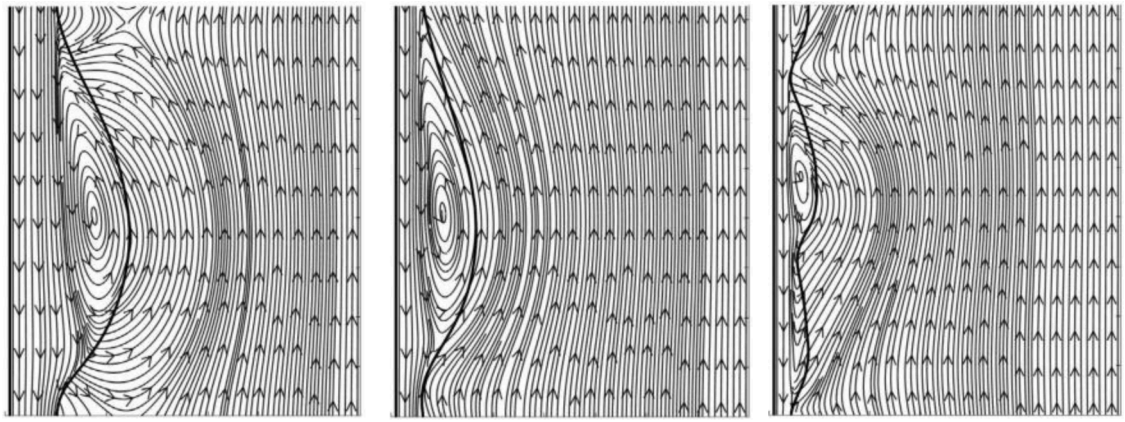

Fig. 8. Snapshots of streamlines with respect to an observer moving with about the interface wave velocity; from left to right, water holdup fraction α_w is 0.44, 0.29, and 0.17.

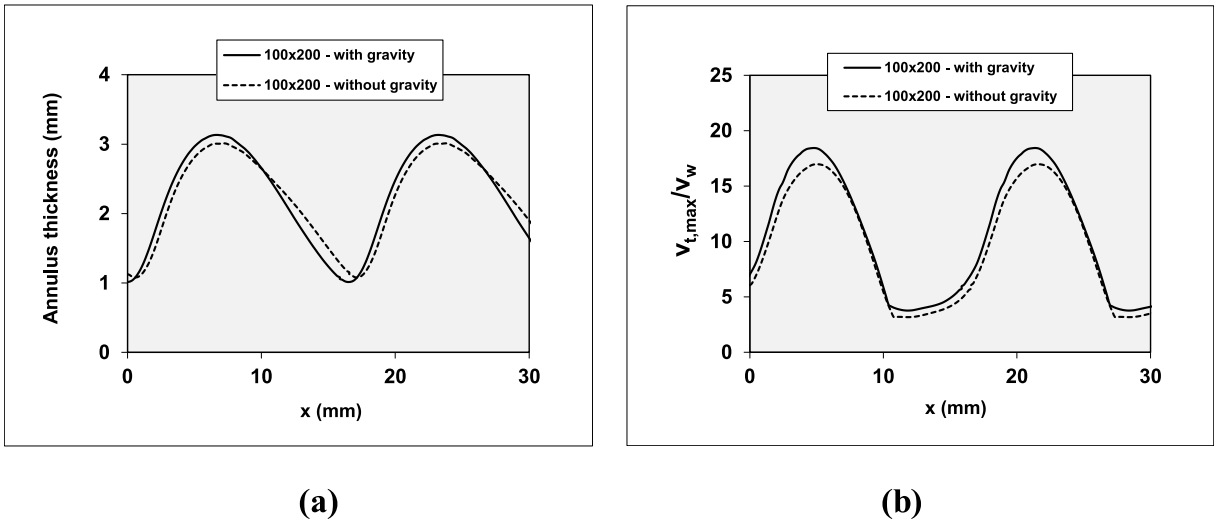

Fig. 9. RANS results with and without gravity for (a) annulus thickness, and (b) maximum turbulent viscosity; water hold-up fraction α_w= 0.29, oil viscosity is μ_o= 0.75 Pa s, section length L= 16.6 mm, frictional pressure drop is 400 Pa/m.

provide many details on the waves. Therefore, the present study is mainly focused on the comparison with the DNS. As Kim & Choi have clearly demonstrated grid-independence of their results, the DNS are thought to be fully representative for the physical reality, and can thus be used for a true validation of the RANS approximations.

The RANS simulations used in this section for comparison were ob-

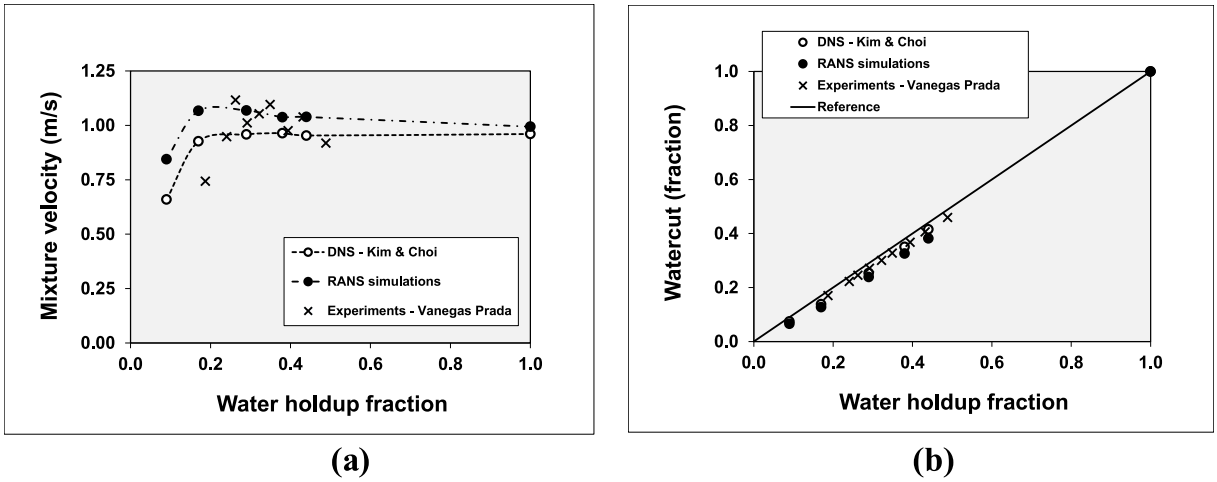

Fig. 10. Comparison of (a) mixture velocity, and (b) watercut, as obtained from RANS, DNS, and experiments; fixed frictional pressure drop of 400 Pa/m and variation of water holdup fraction. The reference line in (b) denotes equal fractions for watercut and water holdup.

tained with a pipe section length L=16.6 mm, an oil viscosity of μo=0.75 Pa s, and an imposed frictional pressure drop of 400 Pa/m. The prescribed water holdup rate was varied. Fig. 10 compares the resulting mixture velocity and watercut with the DNS simulations of Kim & Choi. For the mixture velocity we also compare with the experimental values by Vanegas Prada. RANS predictions for the mixture velocity are about 10% higher than the DNS results. For example at α_w =0.29, RANS gives a mixture velocity of 1.07 m/s, and DNS of 0.96 m/s. For the same water holdup fraction, the RANS value for the watercut is close to the DNS value; in fact the RANS watercut is slightly lower than the DNS value. For example at α_w =0.29, RANS gives a watercut of 23.9% and DNS of 25.4%. This also implies that at the same watercut, RANS will give a higher water holdup fraction (i.e. more water accumulation) than DNS.

4.1. Fanning friction factor

The Fanning friction factor is a dimensionless presentation of the (frictional) pressure drop: $f_W = -\left(\frac{dp}{dx}\right)_{fric}\frac{R}{\rho_w U_m^2}$. Fig. 11a shows the Fanning friction factor for different watercuts, as obtained with RANS and DNS for a fixed frictional pressure drop of 400 Pa/m. From the experiments by Vanegas Prada, those points were selected that have a frictional pressure drop of (about) 400 Pa/m. The RANS predictions for the Fanning friction factor are typically about 18% lower than the DNS values (for watercut fractions in the range 0.1 to 0.5). This means that the same pressure drop (like 400 Pa/m) gives about 18/2 = 9% higher mixture velocity with RANS than with DNS.

There is a fair agreement for the predicted Fanning friction factor and the measurements by Vanegas Prada. When dividing the Fanning friction factor by its value found with water only flow (at the same 400 Pa/m frictional pressure drop), which defines the friction factor ratio as shown in Fig. 11b, it turns out that this ratio is almost equal to 1 for all watercuts (except for the lowest values where the water annulus relaminarizes). This is particularly true for the DNS results.

4.2. Hold-up ratio

The hold-up ratio h shown in Fig. 12 is a measure of the relative water accumulation or of the apparent slip between the oil and water (difference in bulk oil and water velocities). For the 4 higher watercut values used in the DNS (with turbulent water annulus) the RANS prediction for the hold-up ratio is about 12% higher than the DNS prediction. Thus the water accumulation effect is larger in RANS than in the DNS, or: there is more apparent slip between the oil and water in the RANS simulations than in the DNS. The figure also includes a DNS curve and a RANS curve denoted as the "water equivalent" hold-up ratio. This curve is found by considering water-only pipe flow, which is "artificially" splitted in a core and annulus (while they still have same properties for viscosity and density). The watercut and hold-up ratio are now referring to the annulus part of the single-phase RANS results; here the watercut is determined by integrating the DNS or RANS velocity profile in the annulus to give the water flow rate in the annulus, and divide this by the total flow rate through the pipe. This shows that there is relatively much water accumulation (or more apparent slip) close to the pipe wall for low watercut, where water is slowed down due to the wall presence. In fact, this means that the increase in hold-up ratio found for decreasing watercut in the DNS and RANS for the configuration of Kim & Choi can (at least) partly be explained from this natural accumulation effect.

4.3. Water annulus

The values of the temporally and spatially averaged streamwise water velocity in the annulus, as obtained with DNS and RANS, are compared in Fig. 13. The average velocity is made dimensionless with the shear stress velocity u_τ, and the distance to the pipe wall is made dimensionless with ν_w/u_τ. The profile in Fig. 13a shows the averaged water velocity ($u_{w,av}$), whereas Fig. 13b shows the average water velocity multiplied with the average local water holdup fraction (this product is denoted by $u^*_{w,av}$):

$$u_{w,av}* = \frac{\int\int\int u(x,r,t)\ \alpha_w(x,r,t)\ dxdt}{\int\int\int dxdt} = \frac{\int\int\int u(x,r,t)\ \alpha_w(x,r,t)\ dxdt}{\int\int\int \alpha_w(x,r,t)\ dxdt}\cdot\frac{\int\int\int \alpha_w(x,r,t)\ dxdt}{\int\int\int dxdt} = u_{w,av}.\alpha_{w,av} \tag{25}$$

The higher peak for the water velocity for RANS compared to DNS is consistent with the about 10% higher total flow rate (with about the same watercut, namely 23.9% versus 25.4%) found in RANS than in DNS (using an imposed frictional pressure drop of 400 Pa/m and an imposed water holdup fraction of 0.29).

Fig. 14a shows the temporally- and spatially averaged value of the local water holdup fraction, as function of the radial coordinate in the pipe. The imposed overall water holdup fraction is 0.29. Shown are the results with DNS and RANS. For the latter, both the 2D axisymmetric as the 1D results are given. The 1D results are obtained by choosing a very short pipe section, such that all waves are suppressed. Due to the absence of waves the local water holdup fraction abruptly changes from 0 to 1, when the local radius r (scaled with the pipe radius R) becomes larger than $\sqrt{(1-0.29)} = 0.84$. Due to the interface waves, DNS and

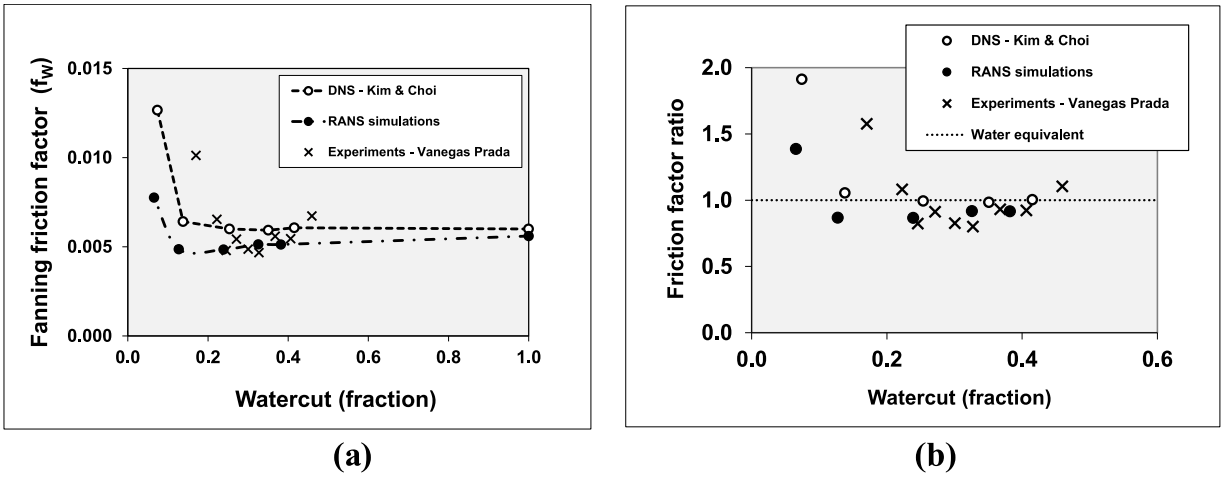

Fig. 11. Comparison of friction factor with RANS (as obtained with a 16.6 mm pipe section length), experiments and DNS as function of the watercut for a fixed frictional pressure drop of 400 Pa/m; (a) Fanning friction factor, (b) friction factor ratio.

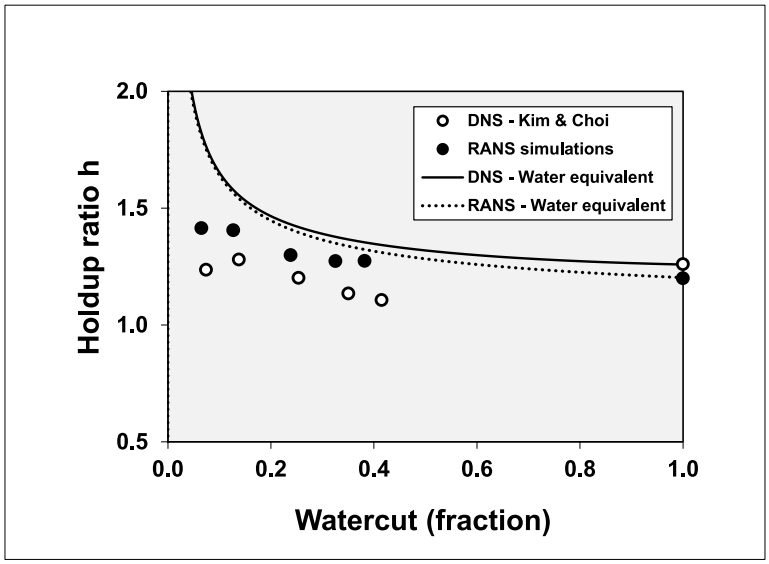

Fig. 12. Comparison of the hold-up ratio obtained with RANS and DNS as function of the watercut for fixed frictional pressure drop of 400 Pa/m.

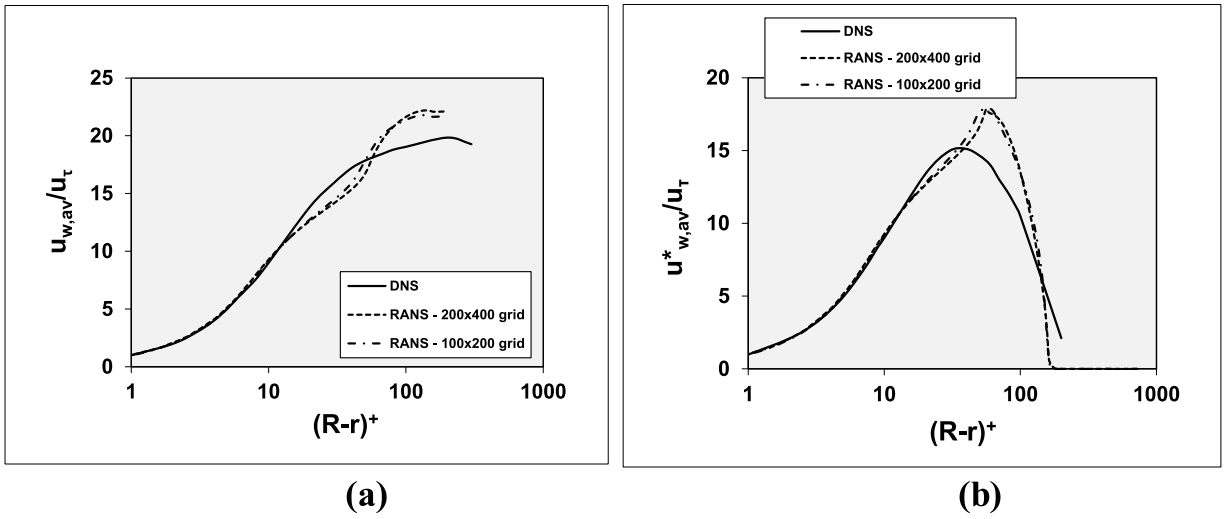

Fig. 13. Average water velocity versus distance from the pipe wall in + units as obtained with DNS and RANS for a water holdup fraction α_w =0.29 and a frictional pressure drop of 400 Pa/m; (a) average water velocity, (b) average of water velocity multiplied with local water holdup fraction.

2D RANS give a more gradual profile of the water holdup fraction. It is also clear from Fig. 14a that the interface waves can reach a higher amplitude in the DNS than in the RANS simulations.

The regularity of the interface waves can be quantified through determining the probability density function (PDF) of the thickness of the water annulus; see Fig. 14b. RANS (for the base pipe section length L=16.6) mm gives a pdf that corresponds to a fully periodic function. DNS has a pdf that corresponds to a spectrum of waves. Increasing the pipe section in the RANS simulations, e.g. to 3L (see also section 3.2.2), breaks the single wave appearance, and a broader PDF is found, that in Fig. 14b looks more like the pdf found with DNS. The average annulus thickness is 2.17 mm (for both DNS and RANS), which corresponds to the imposed water holdup fraction of 0.29. The standard deviation in the water annulus thickness that can be derived from the PDF in the figure is 1.16 mm for the DNS, 0.70 mm for RANS with the base section length L=16.6 mm, and 0.67 mm for RANS with 3L pipe section length. This can be converted to an effective amplitude of the oscillation though multiplying the standard deviation with the factor $\sqrt{2}$; this gives an average wave amplitude of 1.64 mm for the DNS, 1 mm for RANS with section length L, and 0.95 mm for RANS with section length 3L. The amplitude of 1 mm for RANS with section length L is also clearly visible in the results shown in Fig. 4a. The average amplitude of the oscillations in the water thickness (or in the interfacial waves) is thus significantly larger for DNS than for RANS (1.64 mm versus 1 mm). The amplitude in the RANS results is almost independent of the applied section length.

The PDF of the thickness as shown in Fig. 14 only gives information on the wave amplitude, but not on the wave length. With respect to the latter, Kim & Choi (2018) also present graphs of the energy in the wave numbers (or wave length), and of the convective wave velocity for the wave numbers. For a water holdup fraction α_w = 0.29 the wave velocity is about 1.0 m/s in the DNS, versus 1.11 m/s in the RANS results. The spectra in the DNS show that there is energy in the wave numbers in the range of about 1/R to 10/R, corresponding to wave lengths between 8 mm and 80 mm (this range of wave lengths is also visible in the DNS snapshot of the structure of the oil-water interface shown in Fig. 12 in the paper by Kim & Choi). RANS gives a single wave length of 16.6 mm when the applied section length is 16.6 mm, and an average wave length of about 13 mm to 18 mm if larger pipe sections are used. Going from 1×16.6 mm to 3×16.6 mm in RANS shows that the pure single wave periodicity is slightly broken. Further increasing the length of the

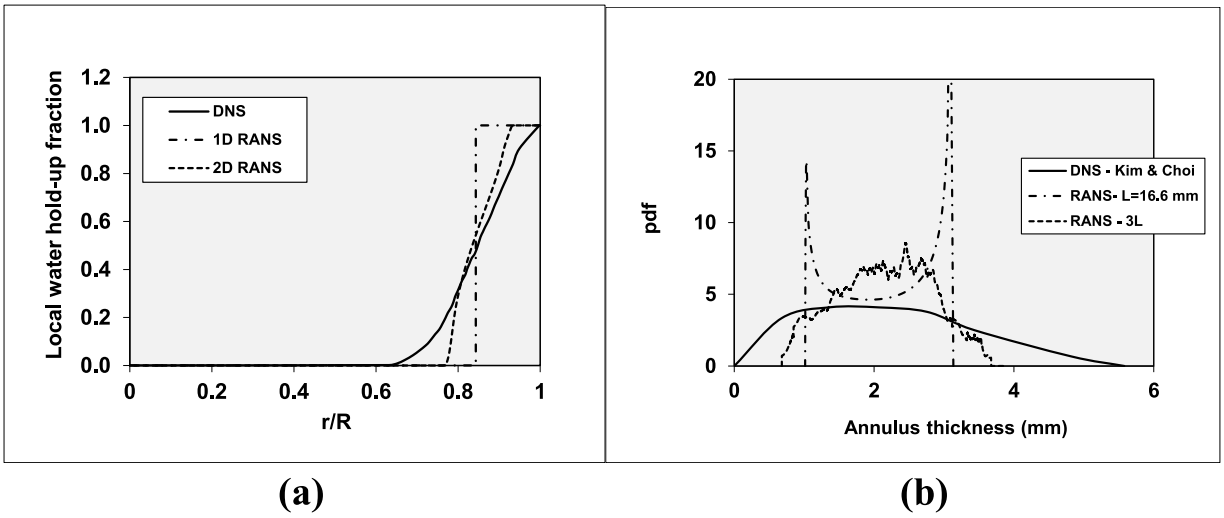

Fig. 14. DNS versus RANS simulation and in DNS for a water hold-up fraction α_w =0.29 and an imposed frictional pressure drop of 400 Pa/m; (a) local water holdup fraction, (b) PDF for the location of the oil-water interface

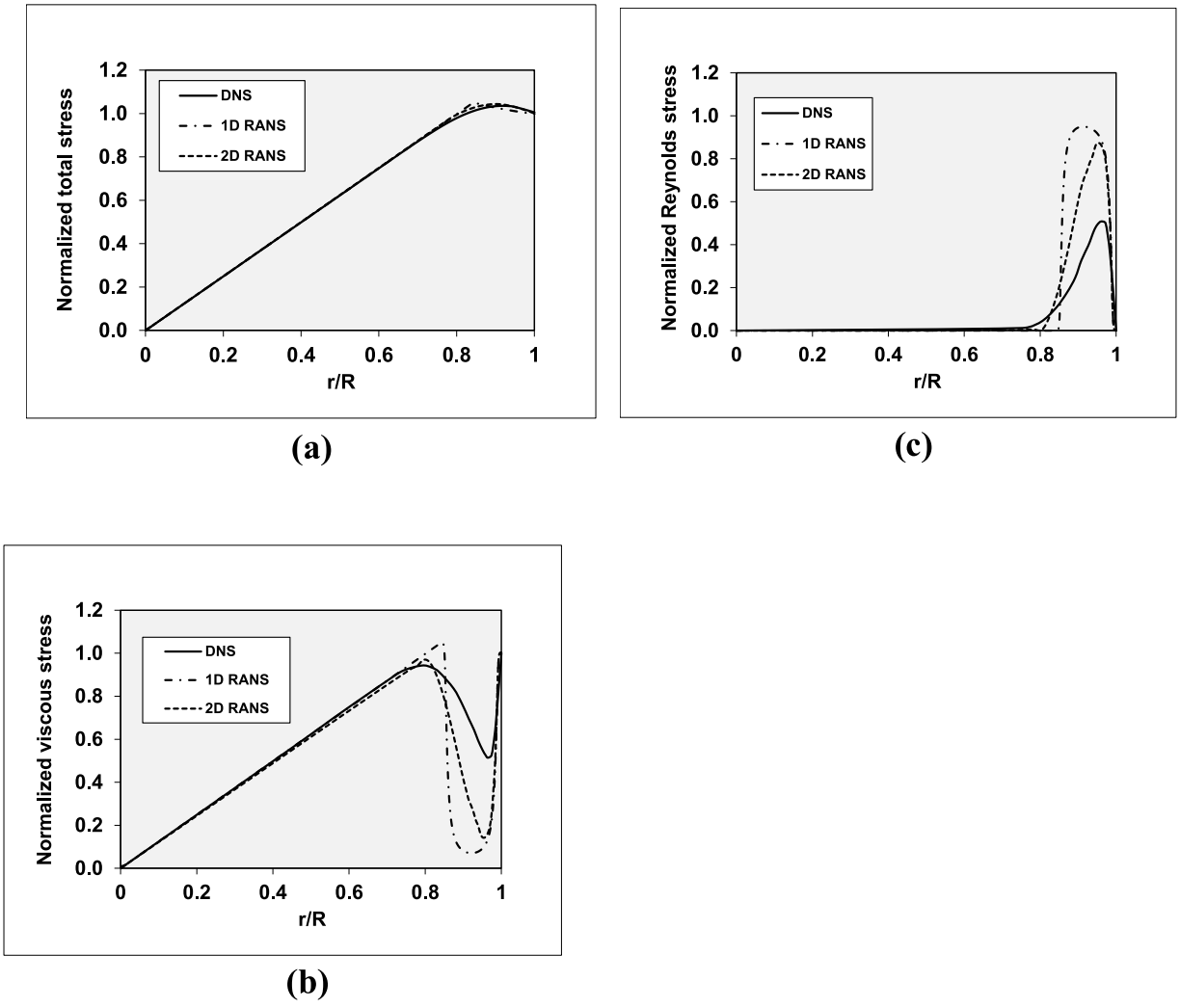

Fig. 15. Profile for the water hold-up fraction and stresses in the RANS simulation and in the DNS for a water hold-up fraction is α_w =0.29 and an imposed frictional pressure drop of 400 Pa/m; (a) total shear stress, (b) viscous stress, (c) Reynolds stress.

computational pipe section may give even more spectrum broadening.

The remarkable difference in the wave spectra between DNS and RANS was also noted by Kim & Choi (2018) when analysing their DNS: "The phase interface amplitude has broadband spectra, which is very different from the observation of the one-wave number peak in laminar core annular flows (Bai et al. 1996, Li & Renardi 1999) and of smooth waves from RANS simulations of turbulent core-annular flows (Ghosh et al. 2010, Ingen Housz et al. 2017, Shi et al. 2017)." The present RANS study shows that choosing the length of pipe section about equal to the most unstable wave length (within the RANS model) will give a travelling wave at the oil-water interface with a single wave length. Increasing the length of the pipe section breaks the single wave appearance, though still gives a dominant with about the length of the originally chosen pipe section (16.6 mm). DNS gives a larger spread of wave lengths, up to sizes of 80 mm which is larger than what is found with RANS. The average amplitude of the waves in DNS (1.64 mm) is larger than in the RANS prediction (1 mm). The difference in wave spectrum may be due to the possibility of azimuthal symmetry breaking in DNS, which is not included in the 2D, axisymmetric RANS.

4.4. Stresses

The simulation results are averaged in time and space to obtain the dependence of the stresses on the radial pipe coordinate. The figures in this section present the stresses after normalization with $\rho_w u_\tau^2$. The averaged total shear stress (as function of the radial coordinate) balances the streamwise pressure force and the gravity force according to:

$$\overline{\tau} = \overline{\rho u_x u_r} - \overline{\mu\left(\frac{\partial u_x}{\partial r} + \frac{\partial u_r}{\partial x}\right)} = \frac{r}{2}\left(-\frac{dp}{dx}\right) - \frac{1}{r}\int_0^r \bar{\rho} g r dr \tag{26}$$

The force due to interfacial tension has been neglected. This formulation is the same as eq. (3.5) in Kim & Choi (2018). The overbar means averaging in the main stream direction and in time. The stress consists of the sum of the viscous stress and the Reynolds stress. In the averaging of the RANS results, the Reynolds stress can be split in a contribution that is due to the Reynolds closure in the $k-\varepsilon$ model and a contribution due to the interfacial wave movement. Fig. 15 shows the DNS and RANS results for the total stress (and for the split-up in a viscous stress and Reynolds stress). For RANS, both the results from the 1D simulation (i.e. no interfacial waves) and the 2D simulation (i.e. with waves) are included. The total stress in Fig. 15a can be easily obtained from the two terms on the right-hand side of Eq. (26): the first term is the prescribed pressure drop (with 400 Pa/m frictional pressure drop), and the second term follows from integrating the radial profile of the averaged water holdup fraction shown in Fig. 14a (with a prescribed total average value $\alpha_w = 0.29$). As expected, due to the prescribed pressure drop and water holdup fraction, there is very good agreement in the radial profile of the total stress for DNS and RANS. There is also good agreement between DNS and RANS for the viscous stress in the oil core (Fig. 15b), which is the only contribution to the total stress in the oil core, but differences are larger in the water annulus. The latter is related to the significantly lower Reynolds stress in the turbulent water annulus (Fig. 15c) according to DNS as compared to the RANS results. Fig. 16 shows the split between the turbulent Reynolds stress and the wave contribution to the Reynolds stress, as derived from the RANS results: the wave contribution is much smaller than the turbulent contribution.

To further study the difference in Reynolds stress between DNS and RANS, Fig. 17 gives the comparison for a range of water holdup fractions between 0.17 and 1. The predictions of the total stress are close (Fig. 17a), but the Reynolds stress is significantly lower with DNS than with RANS (Fig. 17b). The latter is true for all considered water holdup fractions, except for the water-only pipe flow (α_w =1), for which there is close agreement. It is illustrative to show the maximum Reynolds stress as function of the shear-based Reynolds number Re_τ (see Fig. 18), which is defined now as $Re_\tau = d^+ = u_\tau d/\nu_w$. Here u_τ is the wall shear velocity and d is the average thickness of the water annulus: $u_\tau = \sqrt{\tau_W/\rho_w}$ and $\frac{d}{D} = \frac{1-\sqrt{1-\alpha_w}}{2}$. Note that here Re_τ is based on d, whereas earlier it was based on the pipe radius R. The maximum simulated value is Re_τ.= 720. According to Jimenez & Moin (1991), who applied DNS to channel flow, a minimum value of about $Re_\tau = 90$ is needed to sustain turbulence in single-phase channel flow (where d is half the channel width). A decreasing water holdup ratio α_w (i.e. decreasing average thickness of the water annulus d) decreases Re_τ, which will thus give turbulence damping if its value drops below the critical value of 90. As shown in Fig. 17, some of the conditions have a value of Re_τ that is close to, or even below, 90. This will give transitional or fully laminar flow. The low-Reynolds number $k-\varepsilon$ model may be less accurate under transitional conditions. This can explain that the $k-\varepsilon$ model in RANS gives more turbulence damping than DNS; the latter will be able (on sufficiently fine numerical grids) to accurately represent both transitional and fully turbulent flow conditions.

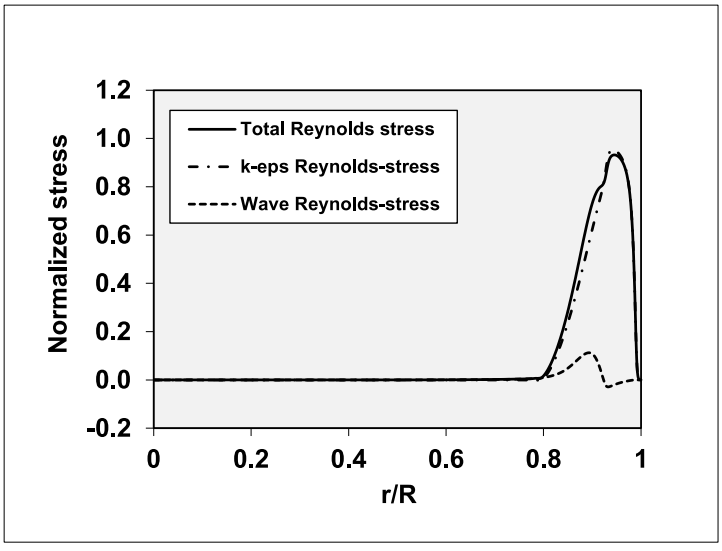

Fig. 16. Radial profile of the composition of the Reynolds stress in the RANS simulation for a water hold-up fraction α_w =0.29 and an imposed frictional pressure drop of 400 Pa/m.

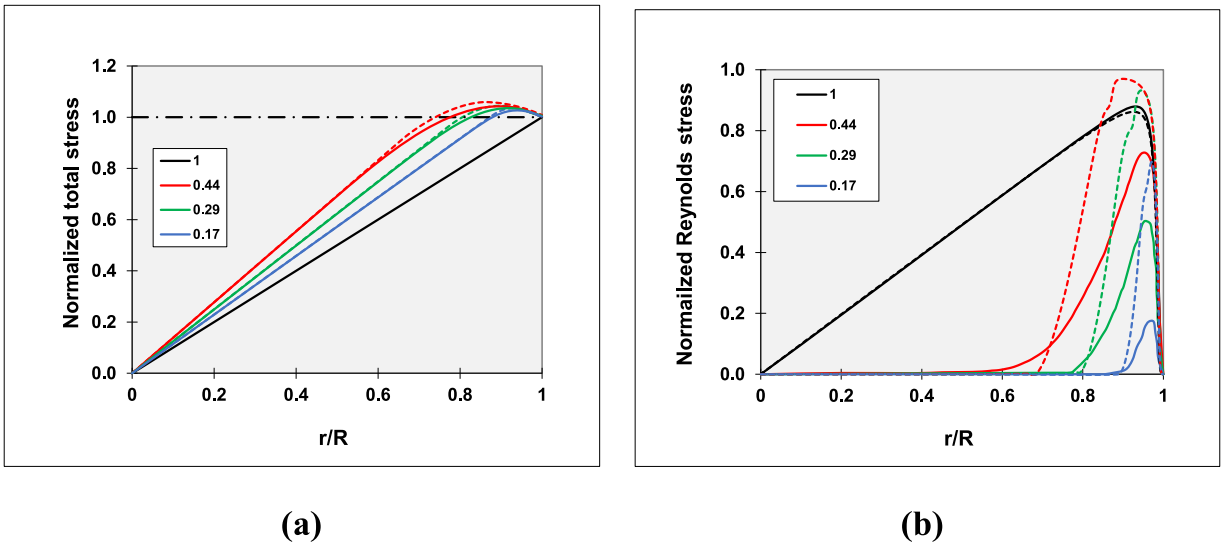

Fig. 17. Radial profile of (a) the total stress, and (b) the (total) Reynolds stress for different values of the water hold-up fraction (values in the legend) and an imposed frictional pressure drop of 400 Pa/m; solid lines denote DNS and dashed lines denote RANS results.

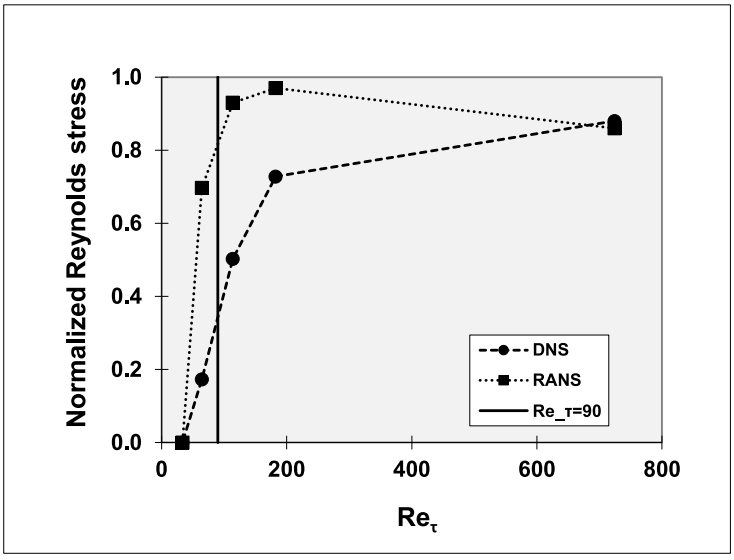

Fig. 18. DNS versus RANS for the maximum Reynolds stress (normalized with $\rho_w u_\tau^2$) as function of the shear-based Reynolds number Re_τ.

5. Conclusions

RANS with the Launder & Sharma low-Reynolds number $k-\varepsilon$ model was used to simulate core-annular flow in the same configuration as was considered by Kim & Choi (DNS) and by Vanegas Prada (experiments). The DNS by Kim & Choi are numerically very accurate and can be used for benchmarking of the RANS turbulence model. The vertical pipe has a diameter of 27.6 mm there is a large ratio between the oil and water viscosities, and the density difference between the water and oil is only small. The frictional pressure drop was fixed at 400 Pa/m and the water holdup fraction was varied.

- The 2D axisymmetric RANS results were shown to be numerically accurate through grid refinement from 100×200 to 200×400 points. The high viscosity ratio used in the DNS and experiments led to the numerical instability in the RANS simulations, and therefore a lower ratio had to be used. Through sensitivity simulations (in which the viscosity ratio was changed) it was shown that the simulation results are not significantly dependent on the viscosity ratio.
- The mixture velocity with RANS is about 10% higher than DNS, and the Fanning friction factor (which is a normalized pressure drop) is about 18% lower. The watercut is only slightly lower with RANS than with DNS, which means that RANS tends to accumulate slightly more water (i.e. same watercut gives more water holdup); the holdup ratio with RANS is 12% higher than with DNS.
- Most RANS simulations were carried out with a pipe section of 16.6 mm which gives a single travelling wave at the oil-water interface with a wave length equal to the pipe section. Increasing the pipe section in RANS gives more irregular wave movement, though the dominant wave is still about 13 to 18 mm. DNS gives a broader spectrum of waves with wave lengths in the range of 8 mm to 80 mm.
- Both RANS and DNS give an almost constant velocity of the interface waves; for example, for a water holdup fraction $\alpha_w = 0.29$, the wave velocity is about 1.11 m/s with RANS and 1.0 m/s in DNS.
- The waves found with RANS are shorter than in DNS. Also, the average amplitude of the waves with RANS is smaller than in DNS. For example, for a water holdup fraction $\alpha_w = 0.29$, the average amplitude of the waves is 1 mm in RANS versus 1.64 mm in DNS. The

smaller wave amplitude in RANS will also give a smaller interfacial stress and herewith more water accumulation (i.e. higher holdup-ratio) than with DNS.
- In the RANS results, the Reynolds stress due to the interfacial waves is much smaller than the turbulent Reynolds stress.
- Decreasing the water holdup fraction (i.e. smaller average thickness of the water annulus) gives significantly less damping of the turbulence in RANS than in DNS (this means that the normalized maximum Reynolds stress in RANS is larger than in DNS). This is due to the complexity of transitional flow and relaminarization that occurs when the shear-based Reynolds is reduced below a critical value of about 90.

Despite the shortcomings of the considered Launder & Sharma low-Reynolds number $k-\varepsilon$ model in RANS, in comparison to DNS, the RANS approach properly describes the main flow structures for upward moving core-annular flow in a vertical pipe, like the travelling interfacial waves in combination with a turbulent water annulus. Arguably, the Fanning friction factor is predicted fairly well, and the prediction of the hold-up ratio is quite good.

CRediT authorship contribution statement

Haoyu Li: Investigation, Writing – original draft. **M.J.B.M. Pourquié:** Supervision, Writing – review & editing. **G. Ooms:** Supervision, Writing – review & editing. **R.A.W.M. Henkes:** Supervision, Writing – review & editing.

Declaration of Competing Interest

The authors declare that they have no known competing financial interests or personal relationships that could have appeared to influence the work reported in this paper.

Data availability

Data will be made available on request.

Acknowledgements

The first author has received a grant from the China Scholarship Council (CSC). Thanks are also due the Netherlands Foundation of Scientific Research (NWO) for supplying the computer time.

References

Bai, R., Kelkar, K., Joseph, D.D., 1996. Direct simulation of interfacial waves in a high-viscosity-ratio and axisymmetric core-annular flow. J. Fluid Mech. 327, 1–34.
Bannwart, A.C., Rodriguez, O.M.H., Carvalho, C.H.M., Wang, I.S., Vara, R.M.O., 2000. Flow patterns in heavy crude oil –water core annular flow. Proceedings of the Engineering Technology Conference of Energy—ETCE 2001, CR-ROM, Feb. 5 –7, Houston, Texas.
Den Toonder, J.M.J., Nieuwstadt, F.T.M., 1997. Reynolds number effects in a turbulent pipe flow for low to moderate Re. Phys. Fluids 9, 3398–3409.
Eggels, J.G.M., Unger, F., Weiss, M.H., Westerweel, J., Adrian, R.J., Friedrich, R., Nieuwstadt, F.T.M., 1994. Fully developed turbulent pipe flow: a comparison between direct numerical simulation and experiment. J. Fluid Mech. 268, 175–210.
Ghosh, S., Mandal, T.K., Das, P.K., 2009. Review of oil water core annular flow. Renew. Sustain. Energy Rev 13, 1957–1965.
Ghosh, S., Das, G, Das, P.K., 2010. Simulation of core annular downflow through CFD – a comprehensive study. Chem. Engng Process. 49, 1222–1228.
Ingen Housz, E.M.R.M., Ooms, G., Henkes, R.A.W.M., Pourquie, M.J.B.M., Kidess, A., Radhakrishnan, R., 2017. A comparison between numerical predictions and experimental results for core-annular flow with a turbulent annulus. Int. J. Multiphase Flow 95, 271–282.
Jiménez, J., Moin, P., 1991. The minimal flow unit in near-wall turbulence. J. Fluid Mech. 225, 213–240.
Joseph, D.D., Bai, R., Chen, K.P., Renardy, Y.Y., 1997. Core-annular flows. Ann. Rev. Fluid Mech. 29, 65–90.
Kim, K., Choi, H., 2018. Direct numerical simulation of a turbulent core-annular flow with water-lubricated high viscosity oil in a vertical pipe. J. Fluid Mech. 849, 419–447.
Launder, B.E., Sharma, B.T., 1974. Application of the energy dissipation model of turbulence to the calculation of flow near a spinning disc. Lett. Heat Mass Transf. 1, 131–138.
Li, H., Pourquié, M.J.B.M., Ooms, G., Henkes, R.A.W.M., 2021. Simulation of turbulent horizontal oil-water core-annular flow with a low-Reynolds number k-ϵ model. Int. J. Multiphase Flow 142, 103744.
Li, H., Pourquié, M.J.B.M., Ooms, G., Henkes, R.A.W.M., 2022. Simulation of turbulent annulus with interfacial waves in core-annular pipe flow. Int. J. Multiphase Flow 154, 104152.
Li, J., Renardy, Y., 1999. Direct simulation of unsteady axisymmetric core–annular flow with high viscosity ratio. J. Fluid Mech. 391, 123–149.
Pirozzoli, S., Romero, J., Fatica, M, Verzicco, R., Orlandi, P., 2021. One point statistics for turbulent pipe flow up to Reτ≈6000. J. Fluid Mech. 926, 355–377.
Shi, J., Lao, L., Yeung, H., 2017. Water-lubricated transport of high-viscosity oil in horizontal pipes: The water hold-up and pressure gradient. Int. J. Multiphase Flow 96, 70–85.
Shi, J., Gourma, M., Yeung, H., 2017. CFD simulation of horizontal oil-water flow with matched density and medium viscosity ratio in different flow regimes. J. Petrol. Sci. Eng. 151, 373–383.
Vanegas Prada, J.W., 1999. Estudo experimental do escoamento anular óleo-áqua ("core flow") na elevação de óleos ultraviscosos. University of Campinas, Brazil. Master Thesis.
Vanegas Prada, J.W., Bannwart, A.C., 2001. Modeling of vertical core-annular flows and application to heavy oil production. Trans. ASME 123, 194–199.
Wu, X., Moin, K., 2008. A direct numerical simulation study on the mean velocity characteristics in turbulent pipe flow. J. Fluid Mech. 608, 81–112.
Wu, X., Baltzer, J.R., Adrian, R.J., 2012. Direct numerical simulation of a 30R long turbulent pipe flow at R^{+}=685; large- and very large-scale motions. J. Fluid Mech. 698, 235–281.
Zaragola, M.V., Smits, A.J., 1998. Mean flow scaling in turbulent pipe flow. J. Fluid Mech. 373, 33–79.